Measurement and effects of polarization fields on one-monolayer-thick InN/GaN multiple quantum wells

Lin Zhou,[1,5,*] E. Dimakis,[2] R. Hathwar,[3] Toshihiro Aoki,[4] David J. Smith,[1] T. D. Moustakas,[2] S. M. Goodnick,[3] and Martha R. McCartney[1]

[1]*Department of Physics, Arizona State University, Tempe, Arizona 85287, USA*
[2]*Department of Electrical and Computer Engineering, Boston University, Boston, Massachusetts 02215, USA*
[3]*School of Electrical Computer and Energy Engineering, Arizona State University, Tempe, Arizona 85287, USA*
[4]*LeRoy Eyring Center for Solid State Science, Arizona State University, Tempe, Arizona 85287, USA*
[5]*Division of Materials Science and Engineering, Ames Laboratory, USDOE, Ames, Iowa 50011, USA*

(Received 28 December 2012; published 25 September 2013)

Polarization fields associated with one-monolayer-thick InN/GaN multiple quantum wells (MQWs) cause shifts of the photoluminescence peak that depend on the GaN barrier layer thickness. Diffraction contrast and aberration-corrected scanning transmission electron microscopy show that the InN QWs are well defined and coherently strained. Mapping of electrostatic potential using off-axis electron holography shows that the electric fields inside the GaN barriers decrease from ∼0.7 to ∼0.2 MV/cm as the barrier layer thickness increases from 5 to 20 nm. Atomistic tight-binding calculations agree closely with experiment, and confirm that changes in optical emission of these III-nitride quantum wells result from changes in the spontaneous and piezoelectric polarization fields in the InN quantum wells and the GaN barrier layers. Overall, this QW system provides the basis for InN-based light-emitting devices operating across a useful band of wavelengths at room temperature.

DOI: 10.1103/PhysRevB.88.125310 PACS number(s): 78.66.Fd, 31.15.aq, 61.05.jp

I. INTRODUCTION

Indium nitride (InN) is the end member of the isomorphous (In, Ga, Al)N series of wurtzite semiconductors which have attracted much attention due to their many different electrical and optoelectronic applications, such as high-electron-mobility transistors (HEMTs) and light-emitting diodes (LEDs). These latter opportunities result from the wide and continuous range of operating wavelengths spanning from ultraviolet to infrared.[1] Moreover, theoretical calculations indicate that ultrathin GaN/InN/GaN quantum wells (QWs) can undergo an inverted band transition and become topological insulators.[2] Insertion of InN multiple quantum wells (MQWs) into LEDs, instead of the more common InGaN ternary or InAlGaN quaternary alloys, could avoid the undesirable effects of phase separation and/or atomic ordering, which occur as the In concentration is increased.[3,4] Recently, an InN/GaN heterostructure consisting of one-monolayer-thick InN wells inserted into a GaN matrix was proposed, and successful growth was reported.[5,6] The growth of near-ultraviolet (384 nm) LEDs based on monolayer-thick InN/GaN MQWs grown by molecular beam epitaxy (MBE) has also been demonstrated.[7] The growth temperature of these monolayer-thick InN/GaN MQWs was 685 °C, significantly higher than normally used for the growth of thick In-polar InN films (400–450 °C).[8] This paper investigates the dependence of optical response of these InN/GaN heterostructures on GaN barrier thickness, which is attributable to the polarization fields in these materials.

III-V nitride semiconductors with the wurtzite structure have large polarization fields along the (0001) direction, which have a significant impact on the optical properties of nitride devices,[1] and affect their potential applications as topological insulators.[2] It has also been recognized that the optical emission of III-nitride quantum wells results from the complex interplay of spontaneous and piezoelectric polarization in the well and barrier layers.[9] Thus, measuring and calculating the electrostatic profiles of one-monolayer-thick InN/GaN MQW structures caused by polarization fields could be important in optimizing device design and operation.

II. EXPERIMENTAL DETAILS

The InN/GaN MQWs were grown by MBE under In-rich conditions at a substrate temperature of 685 °C, keeping the same growth temperature for deposition of InN wells and GaN barriers. Using GaN/sapphire substrates, the growth rate of InN was 0.4 monolayer/s and the nominal deposition thickness of each InN well was slightly greater (∼20%) than 1 monolayer in order to ensure continuous layers. Three specific InN/GaN MQW structures, labeled here as A, B, and C, were targeted for investigation. The widths of the barriers (L_{GaN}) for samples A, B, and C were 5, 10, and 20 nm, respectively.

Cross-sectional samples suitable for TEM and holography observation were prepared by mechanical wedge polishing followed by Ar ion milling at 3 keV using a liquid-nitrogen cold stage. The samples were briefly chemically etched with KOH solution to remove amorphous surface layers created during sample preparation. Diffraction-contrast TEM images were recorded with a JEM-4000EX high-resolution electron microscope operated at 400 keV, while aberration-corrected high-resolution STEM images were recorded with a JEM-ARM200F operated at 200 keV.

III. RESULTS AND DISCUSSION

The emission properties of these InN/GaN MQW structures were investigated by photoluminescence (PL) spectroscopy using the 325-nm line of a He-Cd laser, for optical excitation. Room temperature PL spectra from the MQW structures are shown in Fig. 1. Each spectrum shows two emission peaks,

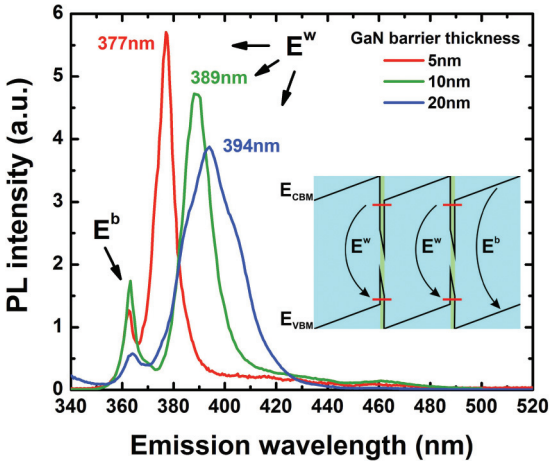

FIG. 1. (Color online) PL spectra of samples A, B, and C recorded at room temperature. The position of E^w shifts to longer wavelength as the barrier thickness is increased. Inset: Quantitative illustration of the band diagram of monolayer-thick InN/GaN QWs and the relevant optical transitions. Blue and green segments correspond to GaN barrier and InN QW layers, respectively.

labeled as E^b and E^w. The former at 363 nm is attributed to radiative recombination of the photoexcited carriers inside the GaN barriers and/or substrate, while the latter is due to radiative recombination inside the InN QWs. The inset schematic illustrates the corresponding optical transitions. That E^w is always stronger than E^b reflects the efficient diffusion and radiative recombination of the photoexcited carriers inside the QWs. E^w shifts to longer wavelengths with increasing L_{GaN}, implying the importance of internal polarization fields, and the resulting quantum-confined Stark effect, in the optical transition energy. Finally, note the width of the E^w emission increases with increasing L_{GaN}. This is possibly due to surface roughening of the thicker GaN barrier layers under nonideal growth conditions (relatively low temperature), which may introduce local InN thickness variations.

Figure 2(a) shows an aberration-corrected STEM image of sample A, oriented in the [110] zone-axis projection. The individual Ga (In) atomic columns are clearly visible as white dots. The average intensity profile along the rectangular region outlined in Fig. 2(a) is plotted in Fig. 2(b). The [In] monolayers are clearly visible and well resolved. No misfit dislocations are observed at the InN/GaN interfaces confirming that the InN QWs are coherently strained with the GaN barriers. Diffraction-contrast image analysis (not shown here) reveals that most of the threading dislocations originating from the GaN template penetrate through the MQWs. Similar microstructure is observed for samples B and C, indicating that all InN layers are coherently strained to the GaN barriers.

Off-axis electron holography is an interferometric electron-microscope technique that provides quantitative access to phase shifts experienced by the incident electron wave front due to interactions with the electrostatic and magnetic potentials of the sample.[10] With its high spatial resolution and sensitivity to variations in electrostatic potential, electron holography has been used to measure the potential profile and charge distribution across nitride heterostructures.[10,11]

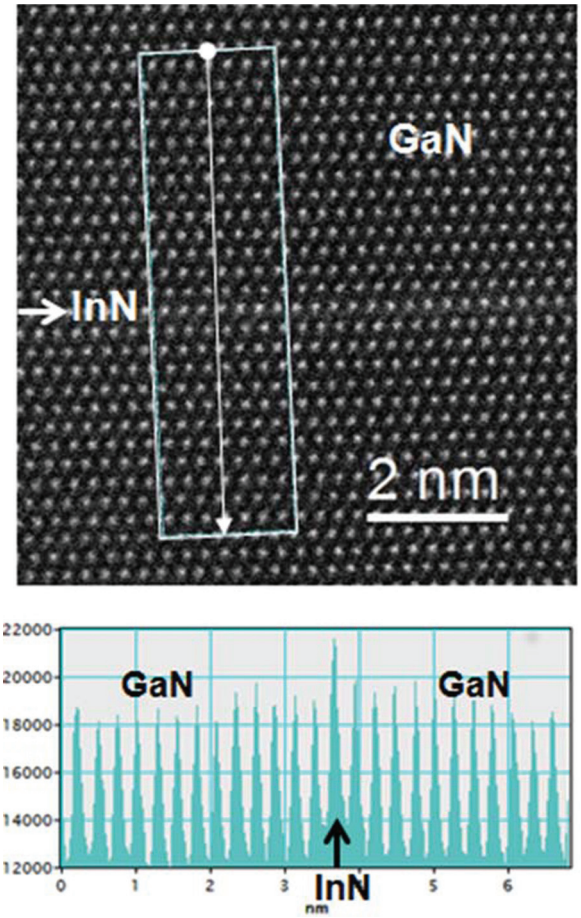

FIG. 2. (Color online) (a) Aberration-corrected high-angle-annular-dark-field STEM image of sample A taken at [110] zone axis. (b) Corresponding intensity line profile from the boxed region of (a). Highest peak (arrowed) corresponds to In atom columns.

In this current study, the electrostatic potential variations of one-monolayer-thick InN/GaN MQWs were measured.

When a (nonmagnetic) TEM sample is not in a strongly diffracting condition and has uniform potential through its projected thickness, then the relationship between electron holography phase shift (ϕ) and local electrostatic potential (V) is given by

$$\Phi(r) = C_E V(r) t(r), \tag{1}$$

where C_E is an energy-dependent constant (0.007 28 rad/V nm for 200 keV electrons) and $t(r)$ is sample thickness.[10] For the GaN barrier layers studied here, the electrostatic potential consists of the mean inner potential of GaN (V_0^{GaN}), and the potential profile due to any electric field in the GaN barrier [$V_E^{\mathrm{GaN}}(r)$]. Thus, the overall phase change in the GaN barriers can be written:

$$\Phi(r) = C_E\left[V_0^{\mathrm{GaN}} + V_E^{\mathrm{GaN}}(r)\right]t. \tag{2}$$

Since V_0^{GaN} is constant, the electric field within the GaN barrier (E^{GaN}) can be calculated by measuring the slope of the potential profile, as extracted from the phase image of a hologram:

$$E^{\mathrm{GaN}} = -d\left[V_0^{\mathrm{GaN}} + V_E^{\mathrm{GaN}}(r)\right]/dr = -dV_E^{\mathrm{GaN}}(r)/dr, \tag{3}$$

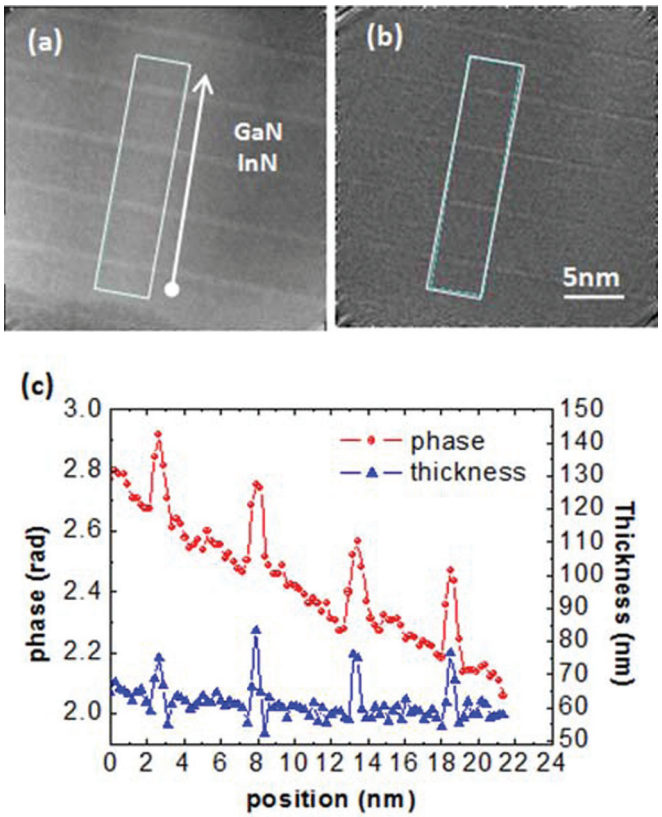

FIG. 3. (Color online) (a) Phase and (b) amplitude images from the reconstructed hologram of sample A. (c) Line profile from the boxed regions of the phase image (red) and calculated thickness profile (blue) from the boxed regions of the amplitude image.

where r is the position along the potential profile, which is taken to be along the growth direction.

Off-axis electron holography was performed using a FEI CM200 FEG TEM equipped with an electrostatic biprism and a CCD camera for quantitative image recording. A biprism voltage of ~125 V was used for hologram recording. Figures 3(a) and 3(b) show the corresponding phase and amplitude images, respectively, from a reconstructed hologram of sample A. The line profile across several MQWs from the rectangular area indicated within Fig. 3(a) is shown in Fig. 3(c). A line profile from the thickness image of the same area, also shown in Fig. 3(c), confirms that the sample has uniform thickness in the region analyzed. A sample thickness of ~60 nm, extracted from the amplitude of the hologram and using the inelastic mean-free path for GaN of 61 nm, was used for calculation of the potential profile.

Figure 4 shows the potential profile of sample A calculated using Eq. (2). The linear slope in potential within the GaN barrier region confirms the presence of the polarization field. Linear fitting of the calculated potential profiles in the three different GaN barrier regions of sample A yielded an average electric field of $\sim 0.71 \pm 0.06$ MV/cm. Similar holography experiments were performed for samples B and C, using the same operating conditions. The electric fields measured for samples B and C were $\sim 0.38 \pm 0.06$ and $\sim 0.20 \pm 0.06$ MV/cm, respectively.

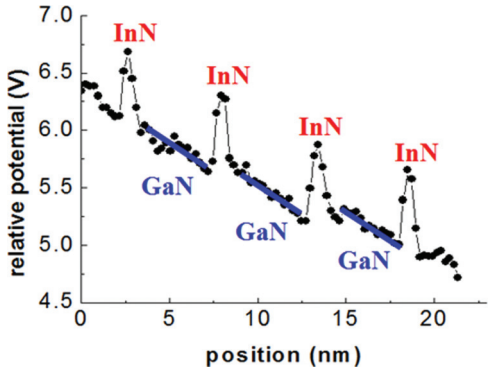

FIG. 4. (Color online) (a) Calculated potential profile across MQW region of sample A. The average GaN electrostatic field (E^{GaN}) obtained by fitting the slope of the potential is $\sim 0.7 \pm 0.06$ MV/cm.

The dependence of E^{GaN} on L_{GaN} can be explained theoretically using relatively simple electrostatic arguments. For a periodic superlattice, E^{GaN} and E^{InN} can be calculated using

$$E^{GaN} = -4\pi L_{InN}\left(P_{tot}^{GaN} - P_{tot}^{InN}\right)/\left(L_{GaN}\varepsilon_{InN} + L_{InN}\varepsilon_{GaN}\right), \quad (4)$$

$$E_{InN} = -4\pi L_{GaN}\left(P_{tot}^{InN} - P_{tot}^{GaN}\right)/\left(L_{InN}\varepsilon_{GaN} + L_{GaN}\varepsilon_{InN}\right), \quad (5)$$

where ε^{InN} (ε^{GaN}) is the InN (GaN) dielectric constant, and P_{tot}^{InN} (P_{tot}^{GaN}) is the sum of the spontaneous and piezoelectric polarization fields in the InN (GaN) layer.[9,12] Based on the high-resolution TEM observations, all InN QWs can be considered as being strained to bulk GaN, so that the piezoelectric polarization in the GaN barrier P_{pz}^{GaN} would be zero. The piezoelectric polarization in the InN QW (P_{pz}^{InN}) can then be calculated using[13]

$$P_{pz}^{InN} = 2\frac{\alpha_{strained}^{InN} - \alpha_{relaxed}^{InN}}{\alpha_{relaxed}^{InN}}\left(e_{31} - e_{33}\frac{C_{13}}{C_{33}}\right), \quad (6)$$

where $\alpha_{relaxed}^{InN}$ and $\alpha_{strained}^{InN}$ are the relaxed and strained (coherently strained to GaN) lattice constants of InN QW. The relevant parameters[9,13,14] and the calculated polarization field are shown in Table I.

The experimental values of E^{GaN} for samples A, B, and C and the corresponding analytical values are shown plotted in Fig. 5, demonstrating reasonably close consistency for all three barriers. One should be cautious with this theoretical treatment of nontrivial quantum structures, such as these monolayer-thick MQW structures. Nevertheless, it is remarkable that a simple electrostatic model could closely simulate the internal polarization fields in these monolayer-thick InN/GaN MQW structures.

TABLE I. Polarization fields, elastic, piezoelectric constants, and dielectric constants used for InN/GaN MQW simulations.[11,13]

	P_{sp} (C/m^2)	P_{pz} (C/m^2)	e_{13} (C/m^2)	e_{33} (C/m^2)	$2C_{13}/C_{33}$	ε (ε_0)
GaN	−0.029	0		0.73		10.5
InN	−0.032	0.152	−0.57	0.97	0.43	13.52

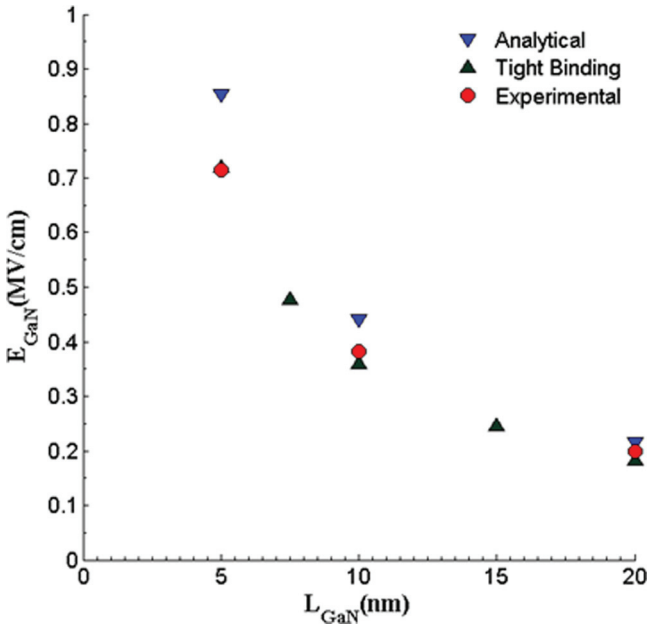

FIG. 5. (Color online) Analytical (inverted triangles), tight-binding (triangles), and experimental (circles) values of electrostatic field E^{GaN}. The measured E^{GaN} values are consistent with the theoretical calculations, confirming that E^{GaN} varies inversely with the barrier thickness.

The electrostatic field within the InN layers, E^{InN}, was also calculated using Eq. (5), and increased slightly with barrier thickness from ~ -12.5 MV/cm for the 5-nm-thick barriers, to ~ -14.0 MV/cm for the 20-nm-thick barriers. Thus, from the simple model described by Eqs. (4) and (5), a stronger quantum-confined Stark effect would be expected for InN QWs that are separated by thicker GaN barriers, which could then result in a redshift of the PL emission, in accordance with the observations. Experimentally, it was not possible from electron holography to determine the corresponding field associated with the InN QWs. Observations with higher spatial resolution could perhaps enable the expected accumulation of sheet charge at the barrier/well interface to be quantified.

In order to better understand the experimental emission spectrum and its dependence on barrier thickness, nearest neighbor sp^3 empirical tight binding (TB) calculations of the heterostructures were performed. The effects of strain and polarization fields were also considered. The band structures of wurtzite materials, specifically GaN, InN, and their alloys, calculated using the TB method, have been shown to be in agreement with experimental data.[15–17] More importantly, transferable TB parameters, which can account for the effects of structural changes on band structure, have been accurately calculated.[18,19] Such a set of parameters is needed to take into account the effects of a coherently strained InN monolayer. The TB parameter set used here was taken from Ref. 19. However, the band gap of InN in Ref. 19 was fitted to an incorrect experimental value of 2 eV. Thus, the onsite energy of the s orbital of In was modified to produce the correct band gap of 0.7 eV,[20] and $E(s,\mathrm{In})$ was changed from -1.373 to -2.985. All other parameters were kept the same.

TABLE II. Calculated (tight binding) and experimental band gaps for different GaN thicknesses.

GaN barrier thickness (actual thicknesses) (nm)	Calculated band gap (eV)	Calculated emission wavelength (nm)	Experimental emission wavelength (nm)
5 (4.92)	3.205	387.5	377
7.5 (7.51)	3.191	389.2	–
10 (10.11)	3.181	390.5	389
15 (14.77)	3.168	392	–
20 (19.96)	3.16	393	394
Bulk (GaN)	3.39	366	364

Due to the InN monolayer, the unit cell of the heterostructure is a supercell comprising many GaN wurtzite unit cells with a distorted GaN-InN wurtzite unit cell. The coherent strain on InN changes the lattice constant of InN in the basal plane to that of GaN (3.189 Å), and to 5.948 Å along the c axis, as calculated using the bulk modulus constants of InN. For a given GaN barrier thickness, and assuming n wurtzite unit cells one on top of another, including the upper most distorted unit cell, the lengths of GaN and InN are calculated using $[(n-1)c + c/2]$, and $c'/2$, respectively, where c is the lattice constant along the z direction of unstrained GaN and c' is the strained lattice constant of InN along the z direction.

The electric fields due to the piezoelectric and spontaneous polarization in GaN and InN are calculated using Eq. (4), and the potential on the atoms of the supercell due to these fields is then incorporated into the TB Hamiltonian. The values for the polarization field for L_{GaN} values of 5, 7.5, 10, 15, and 20 nm are calculated using Eq. (7) and are shown plotted in Fig. 5:

$$V(x) = \begin{pmatrix} x E_{GaN} & \text{for} \quad 0 < x < L_{GaN} \\ L_{GaN} E_{GaN} + (x - L_{GaN}) E_{InN} & \text{for} \quad L_{GaN} < x < L \end{pmatrix}, \tag{7}$$

where L is the total length of the supercell which is $L_{GaN} + L_{InN}$ and x is the distance along the c axis.

The TB calculations exhibit close agreement with the experimental results both for emission wavelength as well as electric field in the GaN buffer layer, as shown in Table II and by comparison with the experimentally derived electric fields in Fig. 5. The closeness of the TB calculations is due to the consideration of strain as well as polarization effects into the TB Hamiltonian. The accuracy of the TB method is greater for larger GaN thicknesses since the effect of the distortion due to the InN monolayer is reduced. For smaller GaN thicknesses, other effects such as excitons, not considered here, could be important.

IV. CONCLUSIONS

In conclusion, one-monolayer-thick InN/GaN MQW structures with different GaN barrier thicknesses were grown at 685 °C by plasma-assisted MBE. Measurement of electrostatic potential profiles using off-axis electron holography showed that the magnitude of the electrostatic field across the GaN barrier layers increased substantially as the thickness of the barrier layer was decreased, in agreement with

theoretical modeling and simulations. Thus, the blue shift of the PL emission peak of these MQW structures with decreasing GaN barrier layer thickness can be understood in terms of changes in strength of the polarization field. These InN/GaN MQW structures would thus be highly promising as the basis for light-emitting devices operating over a range of optical wavelengths, as well as enabling investigation of topological insulator transitions that depend on control of strain due to specific changes in layer and barrier thickness.[2]

ACKNOWLEDGMENTS

The electron holography studies at Arizona State University were partially supported by DOE Grant No. DE-FG02-04ER46168 and the work at Boston University was supported by the DOE Grant No. DE-FG02-06ER46332. We acknowledge use of facilities in the John M. Cowley Center for High Resolution Electron Microscopy at Arizona State University. Acquisition of the JEM-ARM 200F was supported by NSF Grant No. DMR-0821796.

*linzhou@ameslab.gov

[1] H. Morkoç, *Nitride Semiconductors and Devices* (Springer, Berlin, 1999).
[2] M. S. Miao, Q. Yan, C. G. VandeWalle, W. K. Lou, L. L. Li, and K. Chang, Phys. Rev. Lett. **109**, 186803 (2012).
[3] R. Singh, D. Doppalapudi, T. D. Moustakas, and L. T. Romano, Appl. Phys. Lett. **70**, 1089 (1997).
[4] D. Doppalapudi, S. N. Basu, K. F. Ludwig, and T. D. Moustakas, J. Appl. Phys. **84**, 1389 (1998).
[5] A. Yoshikawa, S. B. Che, W. Yamaguchi, H. Saito, X. Q. Wang, Y. Ishitani, and E. S. Hwang, Appl. Phys. Lett. **90**, 073101 (2007).
[6] A. Yoshikawa, S. B. Che, N. Hashimoto, H. Saito, Y. Ishitani, and X. Q. Wang, J. Vac. Sci. Technol. B **26**, 1551 (2008).
[7] E. Dimakis, A. Yu. Nikiforov, C. Thomidis, L. Zhou, D. J. Smith, J. Abell, C.-K. Kao, and T. D. Moustakas, Phys. Status Solidi A **205**, 1070 (2008).
[8] E. Dimakis, E. Iliopoulos, K. Tsagaraki, T. Kehagias, P. Komninou, and A. Georgakilas, J. Appl. Phys. **97**, 113520 (2005).
[9] M. Leroux, N. Grandjean, J. Massies, B. Gil, P. Lefebvre, and P. Bigenwald, Phys. Rev. B **60**, 1496 (1999).
[10] M. R. McCartney and D. J. Smith, Annu. Rev. Mater. Res. **37**, 729 (2007).
[11] M. R. McCartney, F. A. Ponce, J. Cai, and D. P. Bour, Appl. Phys. Lett. **76**, 3055 (2000).
[12] P. Lefebvre, J. Allègre, B. Gil, H. Mathieu, N. Grandjean, M. Leroux, J. Massies, and P. Bigenwald, Phys. Rev. B **59**, 15363 (1999).
[13] O. Ambacher, J. Phys. D: Appl. Phys. **31**, 2653 (1998).
[14] E. Dimakis, E. Iliopoulos, K. Tsagaraki, A. Adikimenakis, and A. Georgakilas, Appl. Phys. Lett. **88**, 191918 (2006).
[15] A. Kobayashi, O. F. Sankey, S. M. Volz, and J. D. Dow, Phys. Rev. B **28**, 935 (1983).
[16] M.-H. Tsai, D. W. Jenkins, J. D. Dow, and R. V. Kasowski Phys. Rev. B **38**, 1541 (1988).
[17] D. W. Jenkins and J. D. Dow, Phys. Rev. B **39**, 3317 (1989).
[18] J.-M. Jancu, R. Scholz, F. Della Sala, and F. Bassani, Appl. Phys. Lett. **81**, 4838 (2002).
[19] T. Yang, S. Nakajima, and S. Sakai, Jpn. J. Appl. Phys. **34**, 5912 (1995).
[20] J. Wu, W. Walukiewicz, K. M. Yu, J. W. Ager, E. E. Haller, H. Lu, W. J. Schaff, Y. Saito, and Y. Nanishi, Appl. Phys. Lett. **80**, 3967 (2002).